Number of stress cycles for fatigue design of simply-supported steel I-girder bridges considering the dynamic effect of vehicle loading

Wei Wang, Lu Deng *, Xudong Shao

Key Laboratory for Wind and Bridge Engineering of Hunan Province, Hunan University, Changsha, Hunan 410082, China

A B S T R A C T

The number of stress cycles (NSC) specified in the AASHTO LRFD bridge design specifications for the fatigue design of steel bridges is evaluated in this paper. A new approach for determining the reasonable number of stress cycles for the fatigue design (NSC_{-FD}) of simply-supported steel I-girder bridges is proposed which takes the dynamic effect of vehicle loading into account. A three-dimensional vehicle–bridge coupled model is developed to simulate the interaction between the bridge and vehicle, in which both the bridge and fatigue load models are adopted from the LRFD code. The equivalent number of stress cycles ($ENSC$), which is calculated based on the fatigue damage accumulation from the dynamic stress time history due to each truck passage, is used for the fatigue analysis of steel girders. Numerical simulations are conducted to study the influence of three important parameters, including the road surface condition (RSC), bridge span length and vehicle speed, on the $ENSC$ of simply-supported steel I-girder bridges. Results show that the RSC has a great impact on the $ENSC$. By considering the cumulative fatigue damage caused by each truck passage under different RSCs and the deterioration process of the RSC during its whole life cycle, simple and reasonable expressions are proposed for calculating the NSC_{-FD} of simply-supported steel I-girder bridges under the given traffic and environmental condition.

© 2015 Elsevier Ltd. All rights reserved.

1. Introduction

The stresses caused by the passage of trucks are a very important factor that determines the fatigue life of steel bridges. The stress range and number of stress cycles (NSC) induced by each truck passage are two key parameters in the fatigue analysis. In the current AASHTO LRFD Bridge Design Specifications [1], a value 1.0 is adopted as the NSC induced by each truck passage for the fatigue design of steel bridges when the bridge is longer than 12.19 m (40 ft) while a value of 2.0 is adopted for bridges no longer than 12.19 m (40 ft). This is based on the study of Schilling [2], in which the NSC is counted when trucks move slowly across simply-supported girders with different spans by ignoring the dynamic effect of vehicle loading. In fact, previous studies have shown that the real stress time history of bridge components and thus the NSC experienced by bridge components can be significantly affected by the dynamic effect of vehicle loading, especially under poor RSC [3–5]. Therefore, the values of 1.0 and 2.0 adopted in the LRFD code [1] for the fatigue design may not truly reflect the

effect of vehicle loading on the NSC experienced by bridge components during the whole life cycle of the bridge.

Within the service life of steel bridges, the dynamic impact of vehicle loading under progressively deteriorated RSC can induce serious fatigue issues for bridge components [4,6,7]. Zhang and Cai studied the effect of RSC on the fatigue life of a steel bridge by using the concept of equivalent fatigue damage in which the equivalent stress ranges and number of stress cycles induced by each truck passage were assembled into one variable [4,5]. They found that the road surface deterioration rate significantly affects the fatigue life of bridge components. However, the effect of each truck passage on the progressive deterioration of RSC and therefore on the accumulative fatigue damage was not considered in their study, which may result in inaccurate prediction of fatigue life of steel bridge components.

In this paper the NSC specified in the LRFD code for fatigue design of steel bridges is evaluated and a new approach is proposed for determining the reasonable NSC_{-FD} of simply-supported steel I-girder bridges that can more rationally consider the dynamic effect of vehicle loading during the whole life cycle of bridges. The structure of this paper is organized as follows. In order to consider the dynamic effect of vehicle loading under different RSCs during the whole life cycle of a bridge, the deterioration process of the RSC under the given traffic and environment condition

* Corresponding author. Tel.: +86 731 88823320.
  E-mail address: denglu@hnu.edu.cn (L. Deng).

is first investigated to obtain the number of truck passages and the time taken for the RSC to deteriorate from one class to the next, for instance, from the "very good" class to the "good" class. Then, a three-dimensional vehicle–bridge coupled model is used to analyze the *ENSC* of the simply-supported steel I-girder bridges under consideration. The influence of three parameters, including the bridge span length, RSC and vehicle speed, on the *ENSC* is investigated based on numerical simulations. In the end, simple and reasonable expressions for the *NSC_FD* of simply-supported steel I-girder bridges are proposed by considering the fatigue damage accumulation resulted from the dynamic vehicle loading under progressively deteriorated RSC during the whole life cycle of bridges.

2. Analytical bridges

The majority of steel bridges in the United States are simply-supported steel I-girder bridges. In this study, five typical steel I-girder bridges with span lengths between 10.67 m (35 ft) and 36.58 m (120 ft) were designed based on the AASHTO LRFD Bridge Design Specifications [1]. The selected range of bridge span is a good representative of the span lengths of simply-supported steel bridges in the United States. All the five bridges are simply-supported bridges and have a roadway width of 9.75 m (32 ft) and a bridge deck thickness of 0.20 m (8 in). Each bridge has five identical girders with a girder spacing of 2.13 m (7 ft). Fig. 1 shows a typical cross section of the bridges. In addition to the end diaphragms used for all five bridges, intermediate diaphragms are also used depending on their span lengths. In the present study, the steel I-girder bridges were modeled with the ANSYS 14.5 program [8]. Fig. 2 shows the finite element model of Bridge 2 (with span length of 16.76 m). The detailed parameters and fundamental frequencies obtained from the modal analysis of the five bridges are summarized in Table 1.

3. Analytical vehicle model

Fig. 3 shows the analytical model of the HS20-44 truck specified in the AASHTO LRFD Bridge Design Specifications [1], which was adopted as the fatigue truck in this study. It should be noted that the distance between the middle and rear axles of the HS20-44 truck for fatigue design is 9.14 m (30 ft). Table 2 summarizes the main parameters of the truck, including the geometry, mass distribution, damping, and stiffness of the tires and suspension systems [9].

4. Vehicle–bridge coupled system

4.1. Equation of motion of the vehicle

The equation of motion for a vehicle can be expressed as follows:

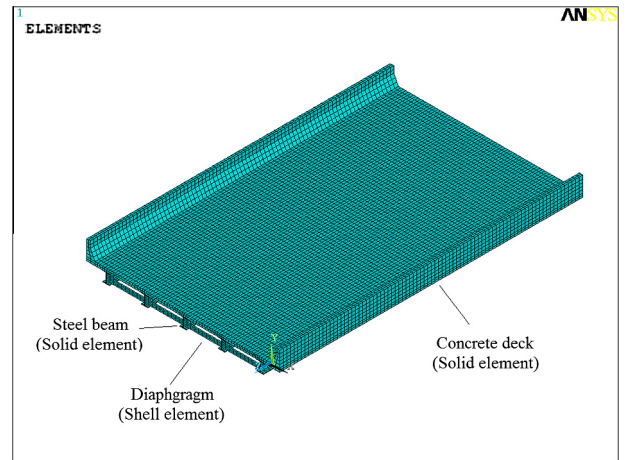$$[M_v]\{\ddot{d}_v\} + [C_v]\{\dot{d}_v\} + [K_v]\{d_v\} = \{F_G\} + \{F_v\} \tag{1}$$

Fig. 2. The finite element model of bridge 2.

Table 1
Detailed properties of the five studied bridges.

Bridge number	Span length (m)	Fundamental natural frequency (Hz)	Girder		Number of intermediate diaphragm
			Cross-sectional area (m²)	Inertia moment of cross-section (10^{-2} m⁴)	
1	10.67	12.40	0.018	0.040	1
2	16.76	8.62	0.020	0.109	2
3	22.86	6.10	0.023	0.219	2
4	30.48	4.39	0.026	0.421	3
5	36.58	3.49	0.028	0.641	4

where $[M_v]$, $[C_v]$ and $[K_v]$ = the mass, damping and stiffness matrices of the vehicle, respectively; $\{d_v\}$ = the displacement vector of the vehicle; $\{F_G\}$ = the gravity force vector of the vehicle; and $\{F_v\}$ = the vector of the wheel-road contact forces acting on the vehicle.

4.2. Equation of motion of the bridge

The equation of motion for a bridge can be written as follows:

$$[M_b]\{\ddot{d}_b\} + [C_b]\{\dot{d}_b\} + [K_b]\{d_b\} = \{F_b\} \tag{2}$$

where $[M_b]$, $[C_b]$ and $[K_b]$ = the mass, damping and stiffness matrices of the bridge, respectively; $\{d_b\}$ = the displacement vector of the bridge; and $\{F_b\}$ = the vector of the wheel-road contact forces acting on the bridge.

4.3. Assembling the vehicle–bridge coupled system

Vehicles traveling on a bridge are connected to the bridge via the wheel-bridge deck contact points. The interaction forces acting on the bridge $\{F_b\}$ and on the vehicles $\{F_v\}$ are actually action and
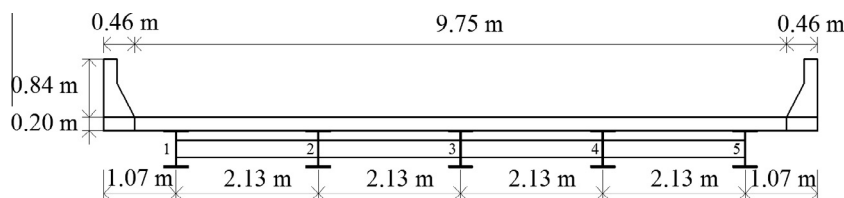

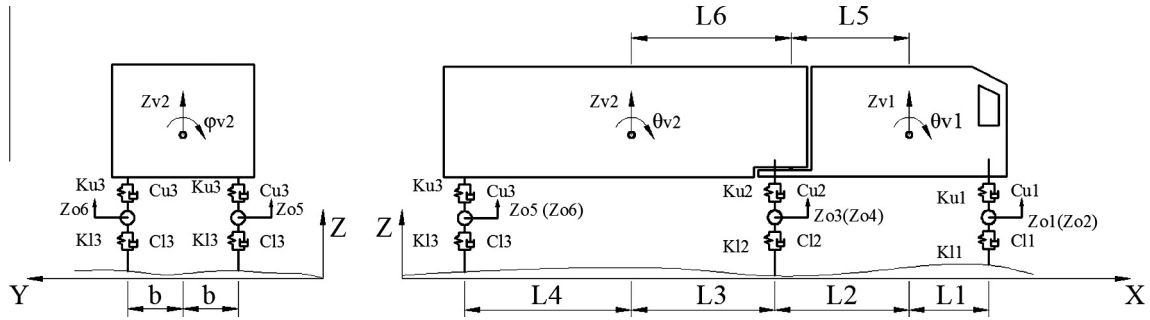**Fig. 1.** Typical cross-section of bridges.

Fig. 3. Analytical model of the fatigue truck.

Table 2
Main parameters of the fatigue truck model used in this study.

Items	Parameters	Values
Geometry	L1	1.698 (m)
	L2	2.569 (m)
	L3	4.452 (m)
	L4	4.692 (m)
	L5	2.215 (m)
	L6	4.806 (m)
	b	1.1 (m)
Mass	Truck body 1	2612 (kg)
	Truck body 2	26,113 (kg)
	First axle suspension	490 (kg)
	Second axle suspension	808 (kg)
	Third axle suspension	653 (kg)
Moment of inertia	Pitching, truck body 1	2022 (kg m²)
	Rolling, tuck body 1	8544 (kg m²)
	Pitching, truck body 2	33,153 (kg m²)
	Rolling, tuck body 2	181,216(kg m²)
Spring stiffness	Upper, first axle	242,604 (N/m)
	Lower, first axle	875,082 (N/m)
	Upper, second axle	1,903,172 (N/m)
	Lower, second axle	3,503,307 (N/m)
	Upper, third axle	1,969,034 (N/m)
	Lower, third axle	3,507,429 (N/m)
Damper coefficient	Upper, first axle	2190 (N s/m)
	Lower, first axle	2000 (N s/m)
	Upper, second axle	7882 (N s/m)
	Lower, second axle	2000 (N s/m)
	Upper, third axle	7182 (N s/m)
	Lower, third axle	2000 (N s/m)

reaction forces existing at the contact points. In addition, the vertical displacement of vehicle body d_v, bridge deflection at the contact point $d_{b\_contact}$, deformation of vehicle spring Δ_L, and road surface profile $r(x)$ have the following relationship:

$$\Delta_L = d_v - d_{b\_contact} - r(x) \tag{3}$$

Based on the displacement relationship and the interaction force relationship at the contact points as described previously, the vehicle–bridge coupled system can be established by combining the equations of motion of both the bridge and vehicle [10], as shown below:

$$\begin{bmatrix} M_b & \\ & M_v \end{bmatrix}\begin{Bmatrix} \ddot{d}_b \\ \ddot{d}_v \end{Bmatrix} + \begin{bmatrix} C_b + C_{b-b} & C_{b-v} \\ C_{v-b} & C_v \end{bmatrix}\begin{Bmatrix} \dot{d}_b \\ \dot{d}_v \end{Bmatrix}$$
$$+ \begin{bmatrix} K_b + K_{b-b} & K_{b-v} \\ K_{v-b} & K_v \end{bmatrix}\begin{Bmatrix} d_b \\ d_v \end{Bmatrix} = \begin{Bmatrix} F_{b-r} \\ F_{v-r} + F_G \end{Bmatrix} \tag{4}$$

where C_{b-b}, C_{b-v}, C_{v-b}, K_{b-b}, K_{b-v}, K_{v-b}, F_{b-r} and F_{v-r} are due to the wheel-bridge contact forces and are time-dependent terms.

Solving Eq. (4) directly can be very time consuming. To simplify the bridge model and therefore save computation effort, the modal

superposition technique can be used. As a result, the displacement vector of the bridge $\{d_b\}$ in Eq. (2) can be expressed as:

$$\{d_b\} = [\{\Phi_1\} \quad \{\Phi_2\}\ldots\{\Phi_m\}]\{\xi_1 \quad \xi_2\cdots\xi_m\}^T = [\Phi_b]\{\xi_b\} \tag{5}$$

where m is the total number of modes used for the bridge; $\{\Phi_i\}$ and ξ_i are the ith mode shape of the bridge and the ith generalized modal coordinate, respectively. Each mode shape is normalized such that $\{\Phi_i\}^T[M_b]\{\Phi_i\} = 1$ and $\{\Phi_i\}^T[K_b]\{\Phi_i\} = \omega_i^2$.

Assuming $[C_b]$ in Eq. (2) to be equal to $2\omega_i\eta_i[M_b]$, where ω_i is the frequency of the ith mode of the bridge and η_i is the percentage of the critical damping for the ith mode of the bridge, Eq. (2) can then be simplified into the following:

$$[I]\{\ddot{\xi}_b\} + [2\omega_i\eta_i I]\{\dot{\xi}_b\} + [\omega_i^2 I]\{\xi_b\} = [\Phi_b]^T\{F_b\} \tag{6}$$

where $[I]$ = unit matrix.

Then, with the transformation in Eq. (6), Eq. (4) can now be written as follows:

$$\begin{bmatrix} I & \\ & M_v \end{bmatrix}\begin{Bmatrix} \ddot{\xi}_b \\ \ddot{d}_v \end{Bmatrix} + \begin{bmatrix} 2\omega_i\eta_i I + \Phi_b^T C_{b-b}\Phi_b & \Phi_b^T C_{b-v} \\ C_{v-b}\Phi_b & C_v \end{bmatrix}\begin{Bmatrix} \dot{\xi}_b \\ \dot{d}_v \end{Bmatrix}$$
$$+ \begin{bmatrix} \omega_i^2 I + \Phi_b^T K_{b-b}\Phi_b & \Phi_b^T K_{b-v} \\ K_{v-b}\Phi_b & K_v \end{bmatrix}\begin{Bmatrix} \xi_b \\ d_v \end{Bmatrix} = \begin{Bmatrix} \Phi_b^T F_{b-r} \\ F_{v-r} + F_G \end{Bmatrix} \tag{7}$$

A Matlab program was developed to assemble the vehicle–bridge coupled system in Eq. (7) and solve it using the fourth-order Runge–Kutta method in the time domain. For more detailed derivation of the vehicle–bridge coupled equation in Eq. (7), readers can refer to [10].

Once the bridge dynamic responses, $\{d_b\}$, are obtained by solving Eq. (7), the stress vector, $[S]$, can then be obtained by the following equation:

$$[S] = [E][B]\{d_b\} \tag{8}$$

where $[E]$ = the stress–strain relationship matrix and is assumed to have constant values over the element; and $[B]$ = the strain–displacement relationship matrix assembled with the x, y, and z derivatives of the element shape functions, following a standard finite element formulation process. It should be noted that Eq. (8) is actually a typical equation to calculate the stress of a finite element based on the nodal displacements of the nodes, the details of which can be easily found in many finite element method books such as [11].

5. Deterioration model of the RSC

5.1. Expression of road surface profile

RSC has a significant influence on the dynamic interaction between the bridge and vehicle. A road surface profile is usually considered to be a zero-mean stationary Gaussian random process and can be generated through an inverse Fourier transformation [12]:

$$r(X) = \sum_{k=1}^{N} \sqrt{2\varphi(n_k)\Delta n} \cos(2\pi n_k X + \theta_k) \qquad (9)$$

where θ_k is the random phase angle uniformly distributed from 0 to 2π; $\varphi()$ is the PSD function (m³/cycle/m) for the road surface elevation; and n_k is the wave number (cycle/m). The following PSD function [13] was used in the present study. The rationale of the chosen PSD function in Eq. (9) has been verified by [12] and also used by other scholars [5,14].

$$\varphi(n) = \varphi(n_0)\left(\frac{n}{n_0}\right)^{-2} \quad (n_1 < n < n_2) \qquad (10)$$

where n is the spatial frequency (cycle/m); n_0 is the discontinuity frequency of $1/2\pi$(cycle/m); $\varphi(n_0)$ is the roughness coefficient (m³/cycle) whose value is chosen depending on the road condition; and n_1 and n_2 are the lower and upper cut-off frequencies, respectively.

5.2. RSC indices

Three indices are usually used to describe the RSC, including the road-roughness coefficient (RRC), present serviceability rating (PSR) and international roughness index (IRI) [15,16]. Both the RRC and PSR categorize the RSC into five classes, namely, very good, good, fair (average), poor, and very poor. However, the RRC is only based on the road profile while the PSR is based on passengers' interpretation of ride quality, which is developed by the AASHTO road test. The International Organization for Standardization [17] adopts the RRC to define the road-roughness classification based on different ranges of RRC listed in Table 3. The IRI, which is based on the average rectified slope (ARS), is also used to define the longitudinal profile of a wheel track [15,18], which is similar to the RRC. Various relationships have been developed between those indices [15,16]. In the present study, the correlation between the IRI and RRC developed by Shiyab [16] was adopted, which can well describe the relationship of the corresponding ranges of the RRC and IRI values. This correlation expression has also been used by other scholars [4]. The correlation is expressed as follows:

$$\varphi(n_0) = 6.1972 \times 10^{-9} \times e^{IRI/0.42808} + 2 \times 10^{-6} \qquad (11)$$

5.3. Progressive deterioration of RSC

Under the combined action of traffic loading and environment corrosion, the RSC will experience progressive deterioration. Different models for the progressive deterioration of RSC have been proposed. Paterson [15] proposed that the IRI values of a road surface at any time since it is opened to traffic can be calculated as:

$$IRI_t = 1.04e^{\eta \cdot t} \cdot IRI_0 + 263(1 + SNC)^{-5}(CESAL)_t \qquad (12)$$

where IRI_t is the IRI value at time t; IRI_0 is the initial roughness value before it is opened to traffic; t is the time in years; η is the environmental coefficient which varies from 0.01 to 0.7 depending on the environmental condition, for instance, dry or wet, freezing or non-freezing; SNC is the structural number which is calculated from

the strength and thickness of each layer in the pavement; and $(CESAL)_t$ is the estimated number of traffic in millions in terms of the AASHTO 80-kN (18-kip) equivalent single axle load at time t. It should be noted that Eq. (12) was initially developed for pavement management systems when initiating the maintenance and rehabilitation of asphalt-surfaced pavements. However, the deterioration of RSC is mainly affected by three factors, namely, initial roughness level, traffic loading and age. Other factors, such as pavement thickness and stiffness, have a smaller influence on the roughness deterioration [16]. Therefore, it was used to analyze the roughness deterioration in this study.

Based on Eqs. (11) and (12), the RRC at any time since being opened to traffic can be predicted with the following equation:

$$\varphi(n_0)_t = 6.1972 \times 10^{-9} \times \exp\{[1.04e^{\eta t} \cdot IRI_0 \\ + 263(1 + SNC)^{-5}(CESAL)_t]/0.42808\} + 2 \times 10^{-6} \qquad (13)$$

In this study, a general environment condition is assumed. The average daily truck traffic (ADTT) and fraction of traffic in a single lane were assumed to be 2000 and 0.85, respectively, as suggested by the LRFD code [1]. According to Shiyab [16], the SNC can then be calculated as 6.19 and η is usually adopted as 0.1 for bridges exposed in general environment condition. Traffic increase was not considered in the present study and thus the $CESAL$ was calculated to be 12.42 for each lane each year [16]. Substituting the values of SNC, $CESAL$ and η into Eq. (13), the time in years taken for the RSC to deteriorate from one class (denoted by the road-roughness coefficient $\varphi(n_0)$) to the next can then be determined. With the assumed ADTT, the number of truck passages, denoted by N_i ($i = 1, 2, 3, 4, 5$), taken for the RSC to deteriorate from one class to the next can then be calculated. For instance, N_1 is the number of truck passages required for the RSC to deteriorate from the class "very good" to the class "good". The calculated time in years (t_i) and number of truck passages (N_i) for the RSC to deteriorate from one class to the next are summarized in Table 4. The proportion of the number of truck passages, $r_i = N_i / \sum N_i$ ($i = 1, 2, 3, 4, 5$), required for the RSC to deteriorate to the next class and the total time in years (T) taken for the RSC to deteriorate to the end of each class since opened to traffic were also calculated.

6. Parametric study

In this section, numerical simulations were performed using a three-dimensional bridge–vehicle coupled model and parametric studies were carried out. The accuracy and reliability of the used bridge–vehicle model was verified in other works [19,20], in which a series of field tests were conducted on an existing slab-on-girder concrete bridge in Louisiana, and the bridge responses, including deflections and strains at the mid-span of the girders, were measured and compared with the bridge responses obtained from the numerical simulations. The field measured results and the numerical results agree with each other very well, in terms of both maximum dynamic responses and the vibration frequencies. The influence of parameters on the interaction of bridge and vehicle has been commonly studied [21–26]. In the present study, three

Table 3
RRC values for five different road-roughness classifications.

Road-roughness classification	Ranges for RRC (m³/cycle)
Very good	2×10^{-6} to 8×10^{-6}
Good	8×10^{-6} to 32×10^{-6}
Average	32×10^{-6} to 128×10^{-6}
Poor	128×10^{-6} to 512×10^{-6}
Very poor	512×10^{-6} to 2048×10^{-6}

Table 4
The number of truck passages and time taken for the RSC to deteriorate to the next class.

Parameter	RSC				
	Very good	Good	Average	Poor	Very poor
N_i	4,113,464	1,156,504	938,321	839,119	768,396
r_i (%)	52.63	14.80	12.01	10.74	9.82
t_i (years)	6.63	1.86	1.52	1.35	1.24
T (years)	6.63	8.49	10.01	11.36	12.60

important parameters commonly considered to have a significant effect on the interaction of bridge and vehicle were investigated to obtain the *ENSC* caused by truck passages, namely, the bridge span length, vehicle speed and RSC.

Table 1 shows the span lengths and other parameters of the five bridges used in this study. A total of seven vehicle speeds ranging from 30 km/h to 120 km/h with an interval of 15 km/h were considered, and five different RSCs based on the ISO [17] were studied, namely, very good, good, average, poor and very poor. Fig. 4 shows the loading case specified in AASHTO LRFD code [1], which was adopted in this study.

To reduce the bias due to the randomly-generated road surface profile, for each specific case with a given bridge span length, vehicle speed and RSC, the vehicle–bridge interaction analysis was set to run 20 times with 20 sets of randomly generated road surface profiles under the given RSC. Then, the average value of the 20 *ENSCs* was obtained and used to investigate the relationship between the parameters and the *ENSC*. Twenty simulations were also considered to be adaquate by other researchers [23].

During the passage of a truck, bridge components can experience complex stress cycles which can be decomposed into the primary stress cycles and one or more higher-order stress cycles [2]. Fig. 5 shows typical static and dynamic stress time history curves at the mid-span of Girder 4 of Bridge 2. The static stress curve was obtained when the fatigue truck crawled across the bridge while the dynamic stress curve was obtained when the truck crossed the bridge at a speed of 45 km/h. The algebraic difference between the maximum and minimum stresses is the stress range for the primary stress cycle, as shown in Fig. 5. The primary stress range at the mid-span of the girder carrying the largest amount of load was selected as the bridge response for calculating the equivalent number of stress cycles in the present study.

Fig. 6 shows the static primary stress ranges at the mid-span of all five girders of each bridge under the loading case considered. It can be easily observed from the figure that the maximum static primary stress range occurs at the mid-span of Girder 4 for all bridges considered. Therefore, the stresses of Girder 4 were used for calculating the *ENSC*. It should be noted that the reason why the static primary stress ranges of Bridge 4 are smaller than those of Bridge 3 on Girders 3 and 4 is that Bridge 4 has a diaphragm right at the mid-span and thus the vehicle loading is more evenly distributed laterally.

Based on the study of Schilling [2], the cumulative fatigue damage due to the complex stress cycles caused by each truck passage can be represented by the fatigue damage of the primary or maximum stress range with the *ENSC* determined from:

$$ENSC = n + \left(\frac{S_{r1}}{S_{rp}}\right)^m + \left(\frac{S_{r2}}{S_{rp}}\right)^m + \cdots + \left(\frac{S_{ri}}{S_{rp}}\right)^m \qquad (14)$$

where n = the number of primary stress cycle induced by each truck passage; S_{rp} = the primary stress range; m = the slope constant of

the *S–N* curve; S_{ri} = the higher-order stress ranges. The slop constant m is approximately equal to 3 for all AASHTO fatigue category details [27].

To illustrate how the RSC affects the *ENSC*, the stress time histories at the mid-span of Girder 4 of Bridge 3 under different RSCs are shown in Fig. 7. It can be observed that the RSC affects the *ENSC*, based on Eq. (14), by affecting the magnitude of the primary stress range, high-order stress ranges and the number of high-order stress ranges simultaneously during the truck passage.
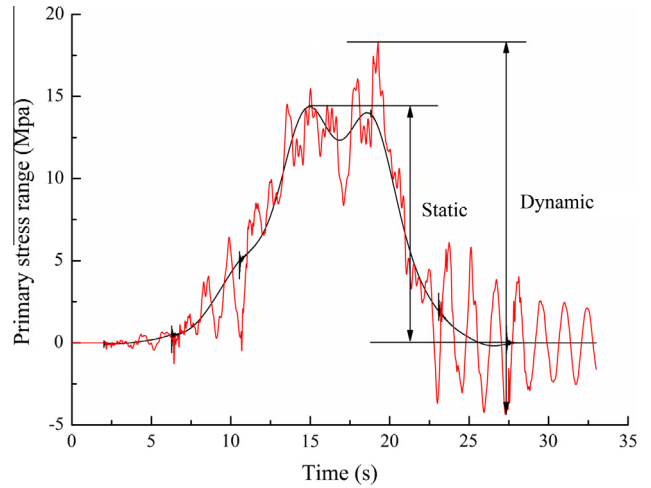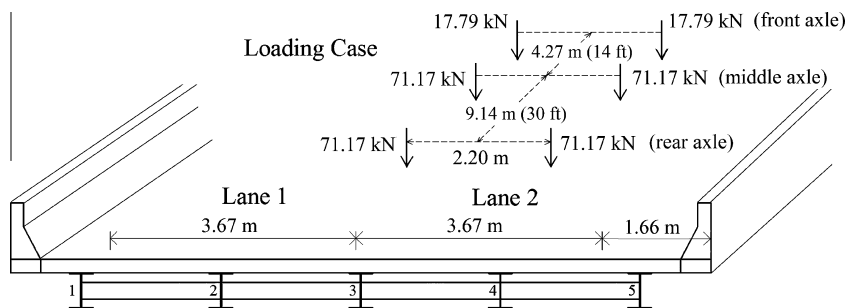

Fig. 5. Illustration of the primary stress cycle.
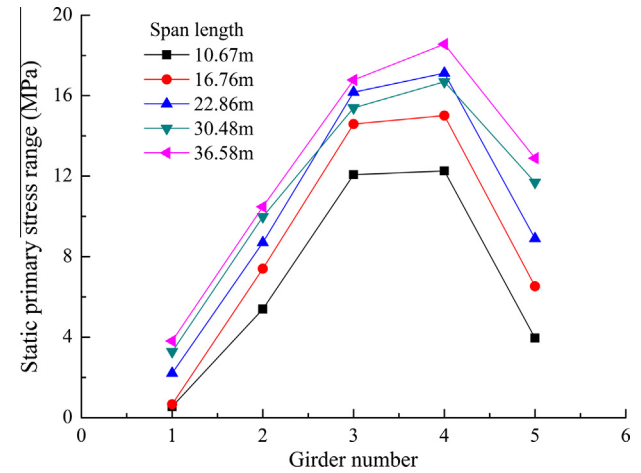
Fig. 6. Static primary stress range at the mid-span of the bridges under the loading case considered.

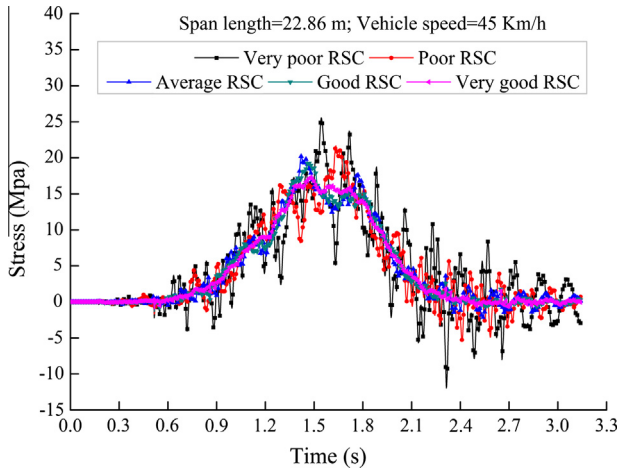**Fig. 4.** Vehicle loading position.

Fig. 7. Stress time histories at the mid-span of Girder 4 of the Bridge 3 under different RSCs when the fatigue truck moves across the bridge.

Since the *ENSC* is greatly affected by the stress-range cutoff threshold, it is necessary to determine a reasonable threshold value when calculating the *ENSC*. Studies have shown that the contribution of stress ranges less than 3.45 MPa (0.5 ksi) to the fatigue life of steel bridges is negligible [28,29]. Therefore, the cutoff threshold for stress-range was chosen to be 3.45 Mpa (0.5 ksi) in this study.

Based on the numerical simulation results, the average *ENSCs* calculated using Eq. (14) for each RSC are plotted against the vehicle speed in Fig. 8 where the results for bridges with different span lengths are plotted separately. As can be seen from Fig. 8, the average *ENSC* can reach as large as 3.0 when the RSC is very poor and can be less than 1.0 when the RSC is very good for the same bridge, demonstrating that the RSC has a significant impact on the *ENSC*. However, an increase of vehicle speed does not necessarily lead to an increase of the *ENSC* due to the fact that an increase of vehicle speed does not necessarily intensify the interaction between the bridge and vehicle, as reported by many other researchers [23,30]. It is noted that the *ENSCs* for the good and very good RSCs in Fig. 8 seem to be very close, which could be due to the following reasons: (1) the magnitudes of the primary stress range under good and very good RSCs are very close; (2) the high-order stress ranges under both good and very good RSCs are not significant and are almost negligible compared to the magnitude of the primary stress range, as can be seen from Fig. 7 where the stress time history of the bridge under a specific load case is provided.

To examine the effect of each parameter on the *ENSC* more clearly, the average *ENSC* is plotted against each of the three parameters separately in Fig. 9. From Fig. 9 it can be easily observed that the average *ENSC* is greatly affected by the bridge span length and RSC. For example, the value of *ENSC* decreases from around 1.55 at the span length of 10.67 m (35 ft) to 1.1 at the span length of 22.86 m (75 ft) and then remains almost a constant when the bridge span further increases. On the other hand, when the RSC changes from "very good" to "very poor", the value of *ENSC* increases from around 1.0 to 1.9.

In order to propose rational values for the number of stress cycles used in the fatigue design of simply-supported steel I-girder bridges, the following steps were taken: firstly, based on the regression analysis on the simulation results, the expressions for predicting the *ENSC* for each RSC are obtained; then, with the consideration of the cumulative fatigue damage caused by each truck passage under different RSCs and the number of truck passages taken to cause the RSC to deteriorate from one class to the

next, the number of stress cycles for the fatigue design of simply-supported steel I-girder bridges were proposed taking into consideration the whole life cycle of the RSC.

Since it has been illustrated that the *ENSC* is highly dependent on the RSC for all bridges considered, it would be very natural to relate the expression of *ENSC* to the RSC. In the present study, the following expressions for predicting the *ENSC* under each RSC are suggested based on a regression analysis:

$$ENSC_i = RSI_i \times \begin{cases} 1.117 + 0.037 \times (22.86 - L) & L < 22.86 \text{ m} \\ 1.117 & L \geqslant 22.86 \text{ m} \end{cases}$$

(15)

where RSI_i = the road surface index, which is taken as 0.87, 0.87, 0.87, 1.23 or 1.65 corresponding to very good, good, average, poor, or very poor RSC, respectively, based on the regression analysis results; and L = the bridge span length.

It should be noted that the reason why vehicle speed is not considered in this expression is that vehicles can usually run with a wide speed range while an increase of vehicle speed does not always cause a monotonic increase or decrease of the *ENSC*. Besides, the influence of vehicle speed on the *ENSC* is smaller compared to the influence of bridge span length and RSC. Therefore, as usually done in the codes, vehicle velocity is not included as a variable in the proposed expressions for predicting the *ENSC*. In addition, it should also be noted that, in real life, drivers are unlikely to drive at high speeds under poor RSC, and therefore it may not be appropriate to calculate the average *ENSC* for poor RSC by taking the average of results for all seven vehicle speeds considered. However, due to the same reasons discussed above, this influence was ignored in this study.

Based on the proposed expressions in Eq. (15), the *ENSCs* of the five bridges studied were predicted for each RSC, as summarized in Table 5.

7. Proposed number of stress cycles for fatigue design

As fatigue failure is resulted from the cumulative damage caused by each truck passage, a reasonable number of stress cycles for fatigue design should consider the effect of each truck passage on the cumulative fatigue damage during the life cycle of the bridge. Based on this consideration, the number of stress cycles for the fatigue design of simply-supported steel I-girder bridges under the traffic and environmental condition suggested by the LRFD code can be calculated using the following expression:

$$\begin{aligned} NSC_{\_FD} &= \sum r_i \times ENSC_i = \sum r_i \times RSI_i \\ &\times \begin{cases} 1.117 + 0.037 \times (22.86 - L) & L < 22.86 \text{ m} \\ 1.117 & L \geqslant 22.86 \text{ m} \end{cases} \end{aligned}$$

(16)

where r_i (i = 1, 2, 3, 4, 5) = the proportion of truck passages needed for each class of the RSC to deteriorate to the next class, as summarized in Table 4.

Based on Eq. (16), the numbers of stress cycles for the fatigue design of the five bridges studied are obtained and summarized in Table 6. It should be noted in Table 6 that two conditions, i.e., Condition "a" and Condition "b", are considered. The only difference between the two conditions is that Condition "a" includes all five RSCs when calculating the $NSC_{\_FD}$ using Eq. (16) while Condition "b" does not include the "very poor" RSC in the calculation. The reason of not considering the "very poor" RSC in Condition "b" is that in real life road maintenance has usually been carried out before the road surface deteriorates to a "very poor" condition. Therefore, Condition "b" may more realistically represent the real situation of the road pavement.
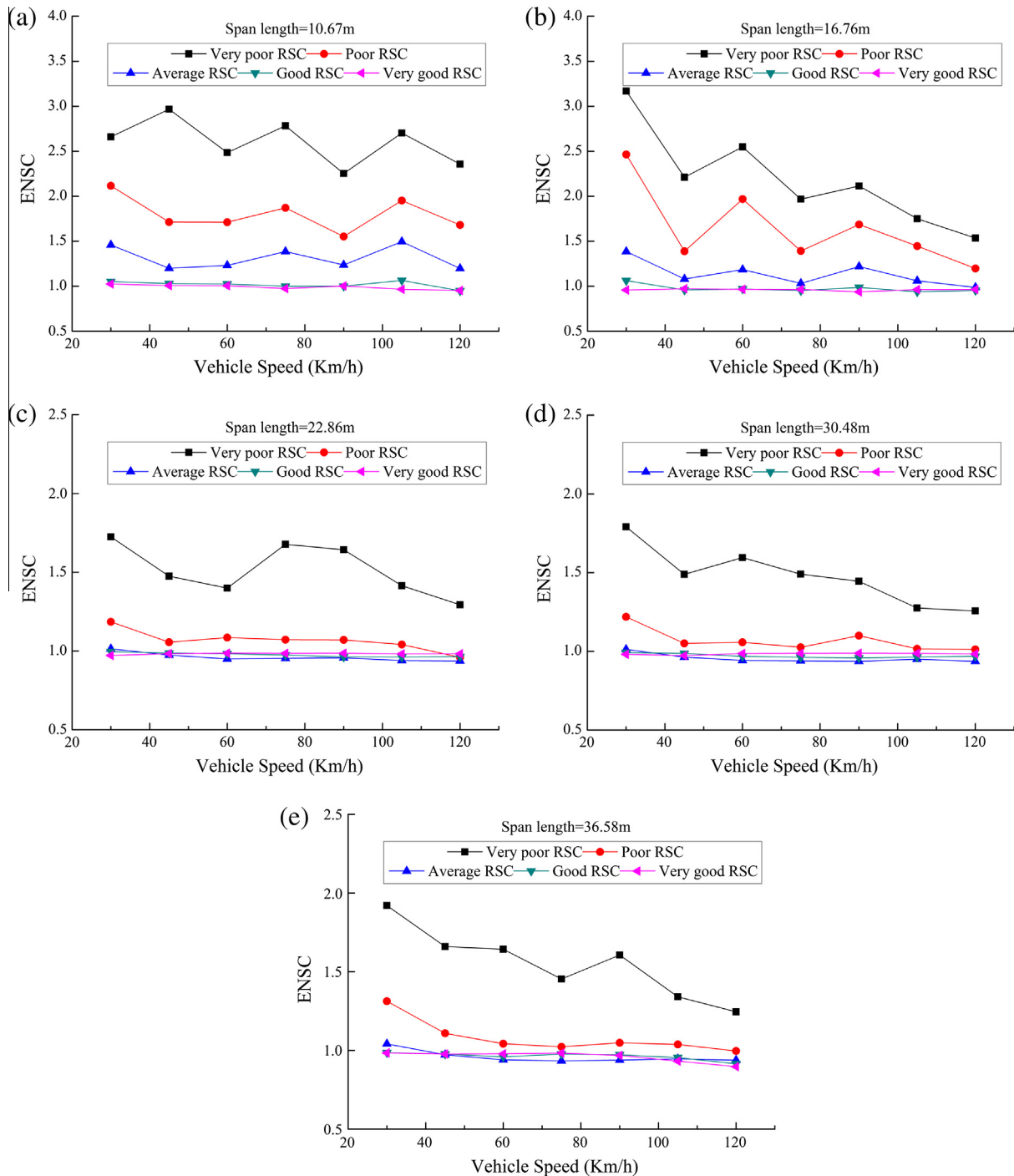
Fig. 8. Variation of ENSC with change in vehicle speed and RSC for different bridges under the loading case considered.

From Table 6, it can be observed that the proposed $NSCs_{-FD}$ for shorter bridges (Bridges 1 and 2) are larger than those for longer bridges (Bridges 3, 4, and 5). In addition, the $NSCs_{-FD}$ under Condition "a" are considerably larger than those under Condition "b", which means that maintaining a good RSC is of great importance in reducing the fatigue damage of bridge components due to the traffic load. Besides, it can be calculated from Eq. (16) that the proposed NSC_{-FD} under Condition "b" equals to 1 when the bridge length is 20.17 m (66 ft). In contrast, in the LRFD code [1] the number of stress cycles for bridge fatigue design is taken as 1 for bridges

longer than 12.19 m (40 ft) and 2 for bridges no longer than 12.19 m (40 ft), respectively. This indicates that the number of stress cycles adopted by the LRFD code for bridge fatigue design may have been underestimated for bridges with length between 12.19 m (40 ft) and 20.17 m (66 ft). Based on the results of this study, it is suggested that a value of 1 may be adopted as the NSC_{-FD} for the main longitudinal components of simply-supported steel bridges with span lengths greater than 22.86 m (75 ft) and a value of 1.5 may be taken for bridges shorter than 22.86 m (75 ft). However, for very short bridges, a larger value such as 2 may be considered.
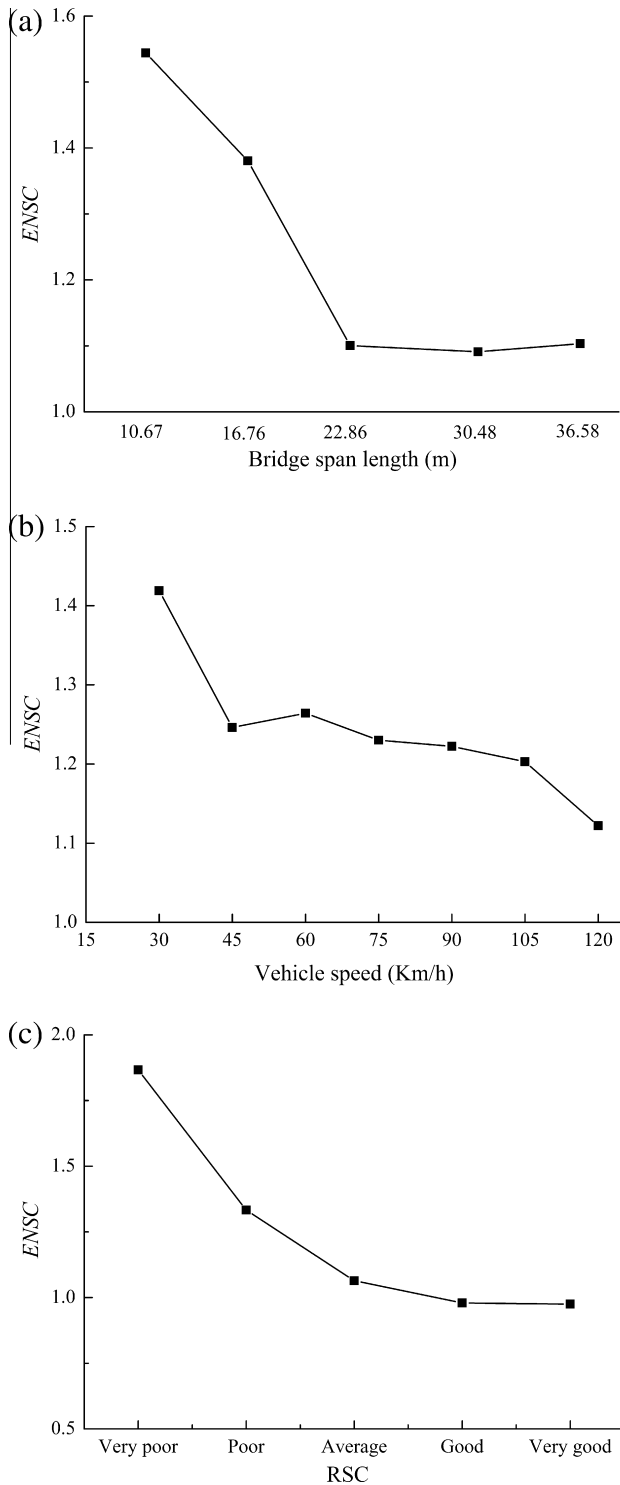
Fig. 9. Variation of the average ENSC with change of each parameter: (a) bridge span length; (b) vehicle speed; (c) RSC.

Table 5
The *ENSC*s of the five bridges.

Bridge no.	RSC				
	Very good	Good	Average	Poor	Very poor
1	1.37	1.37	1.35	1.93	2.59
2	1.17	1.17	1.15	1.65	2.22
3–5	0.97	0.97	0.97	1.37	1.84

Table 6
The $NSCs_{FD}$ for the five bridges studied.

Bridge no.	1	2	3	4	5
Span length (m)	10.67	16.76	22.86	30.48	36.58
NSC_{FD}	1.54[a]|1.29[b]	1.32|1.1	1.10|0.92	1.10|0.92	1.10|0.92

[a] Condition "a": all five RSCs are considered, i.e., very poor, poor, average, good, and very good.
[b] Condition "b": all five RSCs are considered except the "very poor" RSC.

8. Summary and conclusions

In this study the number of stress cycles for fatigue design of simply-supported steel I-girder bridges was studied. Simple and reasonable expressions for calculating the number of stress cycles for the fatigue design of simply-supported steel I-girder bridges were proposed considering the dynamic effect of vehicle loading and the cumulative fatigue damage caused by each truck passage under different road surface conditions during its whole life cycle.

The proposed number of stress cycles calculated with Eq. (16) can be used as supplementation to the AASHTO LRFD bridge design specifications when dealing with the fatigue design of simply-supported steel girder bridges under the assumed traffic and environmental condition. It should be noted that the expression for NSC_{FD} in Eq. (16) was obtained under an ADTT of 2000 and the environmental condition suggested by the LRFD code. However, the proposed approach in the present study is suitable for the fatigue design of steel bridges under different traffic and environmental conditions by adopting different traffic number (*CESAL*) and environmental coefficient (η) in Eq. (13). While this study focused on proposing a new approach for determining the reasonable number of stress cycles for fatigue design of steel bridges and proposed the expressions of NSC_{FD} for simply-supported I-girder bridges with different span lengths, the effects of other parameters, including bridge type, bridge width, etc., on the NSC_{FD} will be the subject of future studies.

Acknowledgments

References

[1] American Association of State Highway and Transportation Officials (AASHTO). AASHTO LRFD bridge design specifications. 6th ed. Washington, D.C.: AASHTO; 2012.
[2] Schilling C. Stress cycles for fatigue design of steel bridges. J Struct Eng 1984;110(6):1222–34.
[3] Rao V, Talukdar S. Prediction of fatigue life of a continuous bridge girder based on vehicle induced stress history. Shock Vib 2003;10(5):325–38.
[4] Zhang W, Cai C. Fatigue reliability assessment for existing bridges considering vehicle speed and road surface conditions. J Bridge Eng 2012;17(3):443–53.
[5] Zhang W, Cai C. Reliability-based dynamic amplification factor on stress ranges for fatigue design of existing bridges. J Bridge Eng 2013;18(6):538–52.
[6] Zhang W, Cai C, Pan F. Nonlinear fatigue damage assessment of existing bridges considering progressively deteriorated road conditions. Eng Struct 2013;56:1922–32.
[7] Zhang W, Yuan H. Corrosion fatigue effects on life estimation of deteriorated bridges under vehicle impacts. Eng Struct 2014;71:128–36.
[8] ANSYS 14.5 [Computer software]. Canonsburg P, Ansys.
[9] Shi X. Structural performance of approach slab and its effect on vehicle induced bridge dynamic response [Ph.D. Thesis]. Baton Rouge (LA): Louisiana State University; 2006.
[10] Deng L, Cai C. Identification of dynamic vehicular axle loads: theory and simulations. J Vib Control 2010;16(14):2167–94.
[11] Logan DL. A first course in the finite element method. 5th ed. Boston: Cengage Learning; 2012.
[12] Huang D, Wang T-L. Impact analysis of cable-stayed bridges. Comput Struct 1992;43(5):897–908.

[13] Dodds C, Robson J. The description of road surface roughness. J Sound Vib 1973;31(2):175–83.
[14] Cai CS, Shi XM, Araujo M, Chen SR. Effect of approach span condition on vehicle-induced dynamic response of slab-on-girder road bridges. Eng Struct 2007;29(12):3210–26.
[15] Paterson WD. International roughness index: relationship to other measures of roughness and riding quality. Transportation Research Record 1084, Transportation Research Board, Washington, DC;1986.
[16] Shiyab A. Optimum use of the flexible pavement condition indicators in pavement management system [Ph.D Thesis]: Curtin University of Technology, Perth, Australia; 2007.
[17] ISO. Mechanical vibration-road surface profiles-reporting of measured data. ISO 8068: (E), Geneva; 1995.
[18] Sayers M, Karamihas S. The little book of profiling: basic information about measuring and interpreting road profiles. Ann Arbor: University of Michigan; 1998.
[19] Deng L. System identification of bridge and vehicle based on their coupled vibration [Ph.D Thesis]: Louisiana State University, Baton Rouge (LA); 2009.
[20] Deng L, Cai C. Bridge model updating using response surface method and genetic algorithm. J Bridge Eng 2009;15(5):553–64.
[21] Chang D, Lee H. Impact factors for simple-span highway girder bridges. J Struct Eng 1994;120(3):704–15.
[22] Yang Y-B, Liao S-S, Lin B-H. Impact formulas for vehicles moving over simple and continuous beams. J Struct Eng 1995;121(11):1644–50.
[23] Liu C, Huang D, Wang T-L. Analytical dynamic impact study based on correlated road roughness. Comput Struct 2002;80(20):1639–50.
[24] Deng L, Cai CS. Development of dynamic impact factor for performance evaluation of existing multi-girder concrete bridges. Eng Struct 2010;32(1):21–31.
[25] Yin X, Fang Z, Cai CS, Deng L. Non-stationary random vibration of bridges under vehicles with variable speed. Eng Struct 2010;32(8):2166–74.
[26] Law SS, Zhu XQ. Dynamic behavior of damaged concrete bridge structures under moving vehicular loads. Eng Struct 2004;26(9):1279–93.
[27] Schilling CG, Klippstein KH. Fatigue of steel beams by simulated bridge traffic. Am Soc Civil Eng 1978;105(1):260–1.
[28] Kwon K, Frangopol D, Soliman M. Probabilistic fatigue life estimation of steel bridges by using a bilinear S–N approach. J Bridge Eng 2012;17(1):58–70.
[29] Kwon K, Frangopol DM. Bridge fatigue reliability assessment using probability density functions of equivalent stress range based on field monitoring data. Int J Fatigue 2010;32(8):1221–32.
[30] Brady SP, O'Brien EJ, Žnidarič A. Effect of vehicle velocity on the dynamic amplification of a vehicle crossing a simply supported bridge. J Bridge Eng 2006;11(2):241–9.